

REVISION OF THE GAMMAGENE EFFECTS OF CARBON AND NITROGEN IN AUSTENITIC STAINLESS STEELS

G. Martos, I. Moreno, R. Sánchez

Research and Testing Centre, ACERINOX, S. A., Spain

Abstract

This research work deals with the recent calculation of the austenite –forming and –stabilizing effects of carbon and nitrogen, the two elements which remained un-reviewed after a thorough revision of the quantitative and qualitative role of the different alloying elements in austenitic stainless alloys which has been carried out by ACERINOX over the last few years.

Three sets of austenitic alloys of the 304 (EN 1.4301), 316 (EN 1.4401) and 304-316 types were prepared as 50 g centrifugally cast, spectrometric buttons which featured the following nominal C and N ranges (in weight %): C - from 0.025 to 0.180, N - from 0.035 to 0.200, and C+N - from 0.060 to 0.240. The base composition of each alloy set was planned to have C and N contents low enough to yield solidification ferrite of some 15 vol.%, which would progressively be reduced from increasing additions of C and N. Each button was systematically examined by ferritescope, light microscopy and electron probe microanalysis. In some cases, analytical electron microscopy was used in order to clarify the nature of the button microstructure.

The investigation has eventually showed that not all the added carbon is put in solution in the solidification structure but it starts precipitating $M_{23}C_6$ for $C > 0.073\%$. Unlike carbon, nitrogen up to the above limit tested is totally dissolved. From these main results, a certain proportion of the bulk C has been considered to take part in the precipitates formation and then eliminated for the calculation of each element gammagene coefficient. A new ferrite forming estimation has been found in which the carbon and nitrogen coefficients are slightly different compared to that commonly used (30 for both elements) in previous models.

Introduction

Not only the equilibrium prediction models but also the constitution diagrams and equations are value tools for the design of more competitive stainless steels, as they allow foreseeing what phases and in which proportions will be present once the solidification process has taken place. These structures determine the steel behaviour trend during their hot working, cold forming, welding, etc.

Several theoretical and/or experimental tools have been developed over the years to predict both the as cast and as welded microstructures of stainless steel alloys. Among the most important experimental ones, those from Schaffler, DeLong and WRC 92 deserve to be mentioned as they are widely used for austenitic steels design purposes. ACERINOX has also addressed this topic and carried out its own works in a twofold direction: that for the prediction of low nickel austenitic stainless microstructures and the revisions of the phase -promoting and -stabilizing effects of the main alloy elements within the standard austenitic grades. In this piece of work the

austenite stabilizing and forming effects of carbon and nitrogen has been quantified for the austenitic stainless steels types 18Cr8Ni and 17Cr11Ni2Mo once the alphagene and gammagene effects of the practical totality of the alloying elements of the common austenitic grades had previously been reviewed.

Materials and experimental

For this specific work, 78 alloys were produced in which, starting from the standard compositions of the 304 (EN-1.4301), 316 (EN-1.4401) and a 304:316 (1:1) mixture, the contents of C and/or N were varied between lower to higher limits of 0.025 and 0.18 wt% respectively.

The minimum contents of C and/or N of the produced alloys were set as to yield a delta ferrite of about 15 wt% in the as-cast condition which should progressively be reduced with further C and/or N additions. In this way it would be possible to assess the gammagene effect of the two studied elements and the possible combined synergies among them.

The alloys were produced as 50g centrifugally cast, spectrometric buttons in a high frequency induction furnace LECO Lifumat Met 3.3 Vac.

The chemical composition of the produced alloys was determined as follows: major elements (Si, Cr, Ni, Mo, Cu and Mn) by XRF, trace elements (W and V) by OES, and C, N and S by Leco analyzers. The nominal weight percent compositions of the produced samples are shown in Tables 1, 2 and 3. Two buttons of each alloy type were manufactured with reproducibility purposes.

Table1. Chemical Composition of 304 type alloys, in weight percent. Solidification delta-ferrite in vol. percent as measured by ferritescope.

	Si	Ni	Cu	Cr	Mo	Co	C	N	V	W	δ
304 B1	0.38	7.50	0.26	18.68	0.48	0.096	0.025	0.035	0.078	0.025	10.84
304 I1	0.36	7.65	0.27	19.31	0.33	0.067	0.059	0.033	0.073	0.016	11.60
304 I2	0.40	7.59	0.26	18.96	0.32	0.074	0.095	0.056	0.068	0.018	6.11
304 I3	0.34	7.47	0.26	19.02	0.32	0.088	0.135	0.040	0.080	0.019	4.72
304 B2	0.38	7.48	0.26	18.78	0.34	0.091	0.179	0.036	0.075	0.020	0.55
304 I4	0.34	7.54	0.26	19.08	0.33	0.073	0.021	0.065	0.073	0.018	12.19
304 I5	0.38	7.56	0.26	18.95	0.34	0.070	0.022	0.111	0.068	0.018	8.94
304 I6	0.33	7.42	0.26	19.05	0.31	0.069	0.021	0.114	0.073	0.016	9.60
304 B3	0.45	7.53	0.26	18.82	0.34	0.081	0.023	0.204	0.082	0.014	0.95
304 I7	0.33	7.44	0.27	18.99	0.31	0.090	0.047	0.056	0.082	0.020	11.37
304 I8	0.39	7.57	0.26	18.89	0.32	0.065	0.065	0.096	0.066	0.017	5.33
304 I9	0.33	7.41	0.26	18.99	0.31	0.089	0.091	0.091	0.081	0.019	5.19
304 B4	0.38	7.52	0.26	18.88	0.33	0.091	0.120	0.123	0.083	0.017	0.51

Table 2. Chemical Composition of 316 type alloys, in weight percent. Solidification delta-ferrite in vol. percent as measured by ferritescope.

	Si	Ni	Cu	Cr	Mo	Co	C	N	V	W	δ
316 B5	0.40	10.54	0.44	18.82	2.21	0.098	0.022	0.033	0.073	0.016	7.91
316 I1	0.43	10.52	0.43	18.82	2.22	0.097	0.058	0.050	0.076	0.021	7.25
316 I2	0.40	10.53	0.44	18.87	2.25	0.096	0.093	0.053	0.075	0.021	4.40
316 I3	0.42	10.54	0.44	18.80	2.27	0.095	0.129	0.049	0.075	0.021	2.42
316 B6	0.41	10.48	0.42	18.58	2.26	0.095	0.181	0.036	0.074	0.020	0.87
316 I4	0.44	10.49	0.43	18.80	2.24	0.075	0.022	0.080	0.071	0.019	8.48
316 I5	0.38	10.53	0.44	18.75	2.28	0.076	0.025	0.111	0.069	0.018	5.79
316 I6	0.40	10.57	0.44	18.85	2.23	0.076	0.022	0.125	0.067	0.019	4.58
316 B7	0.40	10.56	0.43	18.86	2.26	0.091	0.029	0.186	0.071	0.023	1.41
316 I7	0.40	10.42	0.43	18.86	2.23	0.095	0.044	0.069	0.079	0.021	8.24
316 I8	0.40	10.48	0.43	18.88	2.23	0.095	0.067	0.086	0.08	0.020	4.30
316 I9	0.41	10.47	0.48	18.85	2.22	0.095	0.100	0.112	0.079	0.020	2.23
316 B8	0.45	10.55	0.42	18.72	2.22	0.098	0.118	0.124	0.072	0.033	0.19

Table 3. Chemical Composition of 304+316 type alloys, in weight percent. Solidification delta-ferrite in vol. percent as measured by ferritescope.

	Si	Ni	Cu	Cr	Mo	Co	C	N	V	W	δ
SM B9	0.39	9.26	0.33	18.72	1.17	0.088	0.027	0.031	0.078	0.019	7.77
SM I1	0.43	9.17	0.34	18.76	1.12	0.092	0.057	0.053	0.078	0.021	7.23
SM I2	0.41	9.22	0.34	18.96	1.13	0.092	0.093	0.056	0.079	0.022	4.46
SM I3	0.43	9.25	0.34	18.91	1.13	0.090	0.125	0.056	0.078	0.021	1.71
SM B10	0.38	9.26	0.35	18.87	1.12	0.094	0.179	0.036	0.072	0.023	0.41
SM I4	0.41	9.24	0.36	18.88	1.13	0.073	0.022	0.082	0.078	0.018	8.96
SM I5	0.40	9.22	0.36	18.72	1.30	0.070	0.022	0.121	0.073	0.017	5.92
SM I6	0.40	9.17	0.37	18.77	1.13	0.067	0.022	0.137	0.072	0.017	4.07
SM B11	0.41	9.33	0.35	18.88	1.18	0.090	0.031	0.202	0.070	0.023	0.45
SM I7	0.42	9.30	0.35	18.94	1.11	0.097	0.045	0.065	0.078	0.021	7.80
SM I8	0.40	9.30	0.36	19.00	1.11	0.098	0.068	0.088	0.078	0.021	4.25
SM I9	0.36	9.32	0.35	19.14	1.11	0.097	0.087	0.109	0.078	0.021	1.65
SM B12	0.38	9.33	0.35	18.92	1.16	0.099	0.120	0.131	0.078	0.021	0.12

The residual ferrite percentage shown in the previous tables was determined by the magnetic permeability measured by a ferritescope Fischerscope MMS fitted with Permascope probe. The method is based on the fact that, from the magnetic properties of the ferrite and the austenite phases, a direct relationship can be established between the stainless steel magnetic permeability and the ferrite volume percentage which is present in the steel sample.

Once the buttons were chemically characterized, they were all examined by light microscopy, electron probe (EPMA) and, some of them, by transmission electron microscopy (TEM). Both electronic techniques being applied by the SCT of the Universidad de Barcelona. The electron probe microanalysis was performed with a Cameca SX-50 equipment, which determined the composition of a hundred points along a segment contained in the mid plane of each button sample. The presence and nature of the precipitates present in the selected samples were studied in a TEM Hitachi H800 MT fitted with EDX KeVex Quantum.

Exam of the solidification microstructures

Quantifying the gamma-gene effect of carbon and nitrogen in the solidification microstructure involves an in deep assessment of such microstructure in terms of type and amount of the existing constituents (major phases and precipitates). This has been done through optical and electron microscopies and electron probe.

The picture below shows an example of the solidification microstructure of the buttons 304 B1 and 316 B5, which shows the austenitic matrix and a residual interdendritic ferrite content of some 10.84 vol.% and 7.91% vol, respectively.

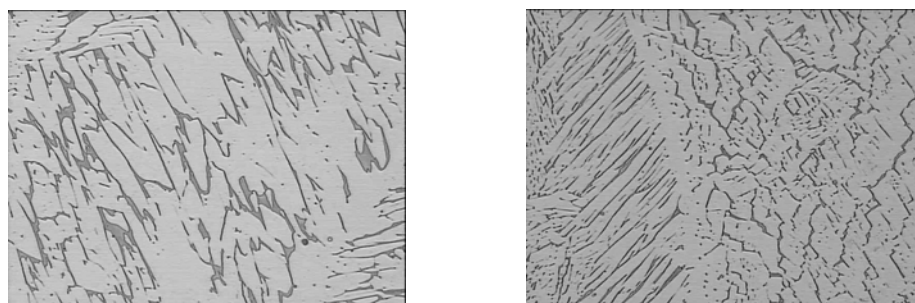


Figure 1. As cast microstructures of the buttons 304 B1 and 316 B5 comprising residual ferrite (10.84%vol and 7.91%vol, respectively) in austenite matrix.

The TEM study allowed to determine the presence of precipitates formed during the solidification process and, in such a case, their crystalline nature. The obtained results for the analysed alloys are summarized in the following table.

Table 4. TEM analysis.

	LECO (weight %)		Precipitate type
	C	N	
304 B1	0.025	0.035	MnCrO ₄
304 B2	0.179	0.036	Cr ₂₃ C ₆ , Fe ₃ C
304 B3	0.023	0.204	MnCrO ₄ , Fe ₃ C
304 B4	0.121	0.123	MnCrO ₄

In the analysed alloys having high carbon contents (304 B2 and 304 B4), carbide precipitates were found. This carbon that is tied up with metals to form precipitates doesn't exert any gammagene effect. Nitride precipitates were not found in any of the analyzed samples.

The quantitative analysis of the C and N in solution in the austenite was done by EPMA. The obtained results for the analysed alloys are collected in Table 5. The C and N values measured by LECO are also shown in this table.

Table 5. EPMA results.

	LECO (weight %)		EPMA (weight %)	
	C	N	C dissolved in γ	N dissolved in γ
304 B1	0.025	0.035	ALL	ALL
304 B2	0.179	0.036	0.073	ALL
304 B3	0.023	0.204	ALL	ALL
304 B4	0.121	0.123	0.072	ALL
316 B5	0.032	0.030	ALL	ALL
316 B6	0.181	0.029	0.075	ALL
316 B7	0.029	0.187	ALL	ALL
316 B8	0.118	0.124	0.075	ALL

As shown in Table 5, all N added to the alloys is dissolved in the austenitic matrix, while only a part of the C added is taken into solution in this phase; the rest of it being found taking part of precipitates. The maximum C content that is able to take into solution the austenite, as to the specific cooling and solidification conditions for this research, is about 0.073wt%.

Therefore, while all the N added can be considered that is exerting an austenite forming and/or stabilizing effect over the entire alloying range of this study, the C only has a gammagene effect up to 0.073wt%, and thus higher C contents will just contribute to form Cr₂₃C₆ and Fe₃C.

Calculation of the carbon and nitrogen gammagene coefficients

For the calculation of the gammagene coefficients of the elements under study, the following reference equation is taken which comes from previous research carried out by ACERINOX:

$$\%Fe\delta = \left(\frac{Cr_{eq} + 18}{Ni_{eq} + 36} + 0.262 \right) \times 161 - 162.1$$

$$Cr_{eq} = Cr + Mo \times (1.15 - 0.33 V^2) + 0.66Si + 0.83W + 2.66V$$

$$Ni_{eq} = Ni + 30 \times (C + N) + 0.27Cu + 0.32Co$$

The above is the so called modified DeLong equation, in which either the gammagene or alphagene power of the element is expressed by a factor that multiplies the relevant element concentration. On the basis of this equation and bearing in mind the obtained results from the TEM and EPMA studies, the following multivariable linear regression, where the C and N powers are established as the unknown variables, is analyzed:

$$\%Fe\delta = \left(\frac{Cr_{eq} + 18}{Ni_{eq} + 36} \right) \times 161 - 162.2$$

$$Cr_{eq} = Cr + Mo \times (1.15 - 0.33 V^2) + 0.66Si + 0.83W + 2.66V$$

$$Ni_{eq} = Ni + X_1 \cdot C + X_2 \cdot N + 0.27Cu + 0.32Co$$

Operating:

$$F = \frac{18 + Cr_{eq}}{36 + Ni_{eq}} = \frac{18 + Cr_{eq}}{36 + X_1 \cdot C + X_2 \cdot N + 0.27Cu + 0.32Co + Ni}$$

$$[36 + X_1 \cdot C + X_2 \cdot N + 0.27Cu + 0.32Co + Ni] = \frac{18 + Cr_{eq}}{F}$$

$$X_1 \cdot C + X_2 \cdot N = \frac{18 + Cr_{eq}}{F} - 36 - 0.27Cu - 0.32Co - Ni$$

$$G = X_1 \cdot C + X_2 \cdot N$$

The obtained regression parameters are shown in Table 6.

Table 6. First multivariable linear regression.

Unknown variable	Value	Error	R ² (n=78)
C	30.9224	0.86027	99.0318
N	28.7202	0.75519	

If the estimated ferrite from the above calculations is plotted against the measured (by ferritescope) ferrite, one can find that there are six results out of the 2σ confidence range:

304 B1, 316 B5, 316 B5d, SM B9, SM B12 and SM B12d (see Figure 2).

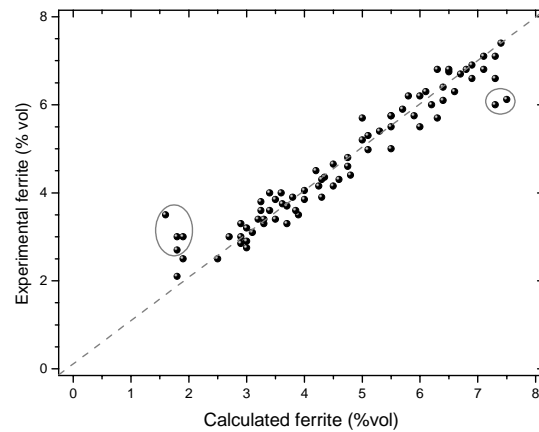


Figure 2. Calculated ferrite vs measured ferrite.

These six values are ruled out and the adjustment calculation has been done again. The obtained results for this new regression are shown in Table 7.

Table 7. Second multivariable linear regression.

Unknown variable	Value	Error	R^2 (n=72)
C	31.0905	0.58522	
N	28.7699	0.50019	99.5643

With this new adjustment, the final equation is found to be:

$$\% \text{Fe}\delta = \left(\frac{\text{Cr}_{\text{eq}} + 18}{\text{Ni}_{\text{eq}} + 36} \right) \times 161 - 162.2$$

$$\text{Cr}_{\text{eq}} = \text{Cr} + \text{Mo} \times (1.15 - 0.33 \text{V}^2) + 0.66\text{Si} + 0.83\text{W} + 2.66\text{V}$$

$$\text{Ni}_{\text{eq}} = \text{Ni} + 31.09 \cdot \text{C} + 28.77 \cdot \text{N} + 0.27\text{Cu} + 0.32\text{Co}$$

Conclusions

In the reported work, the gammagene effects of C and N on the microstructure of common stainless steels have been examined. The investigation has showed that C values higher than 0.073 w% lead to carbide formation. On the other hand, nitrogen up to the above limit considered (0.18 w%) is totally in solid solution. From this main result, the amount of C taking part in the precipitates formation has been removed for the calculation of the element's gammagene coefficient.

A new ferrite formation predicting model, based on that recently updated by ACERINOX, has then been calculated in which carbon and nitrogen coefficients are slightly different compared to that commonly used (30 for both elements) in previous models. The new gammagene coefficients are 31.09 for carbon and 28.77 for nitrogen.

References

- [1] Guiraldenq, P., "Ferrite and Austenite Forming Tendencies of the Principal Alloying Elements in 18Cr-10Ni Stainless Steel". *Revue de Metallurgie, Memoires Scientifiques*, Vol. 64, N° 11, p. 907-939 (1967).
- [2] Potak, M., Sagalevich, E.A., "Structural Diagram for Stainless Steels as Applied to Cast Metal and Metal Deposited During Welding" *Avt. Suarka*, 1972, N° 5, p. 10 - 13.
- [3] Hammar, Ö., Svensson, U., "A guide to the solidification of steels". Jerkontoret, Stockholm (1977).
- [4] Marshall P. "Austenitic Stainless Steels. Microstructure and Mechanical Properties". Ed. Elsevier Applied Science publishers (1984).
- [5] G. Allan. "Castability, solidification mode and residual ferrite distribution in highly alloyed stainless steels". Luxembourg: Office for Official Publications of the European Communities. ISBN 98-827-9302-8. (1997).
- [6] J.F. Almagro, C Luna, J. Botella. "Técnicas de caracterización microestructural de aceros: la microscopía electrónica de barrido con espectrometría EDS. Aplicación al análisis de fases, precipitados e inclusiones". *Avances en ciencias y tecnología del acero inoxidable. 1^{as} Jornadas de Metalurgia de INOX-RED*. Editores J.A. Odriozola y J.Botella. ISBN 84-923464-3-4 p. 319-351. Sevilla .2001.

ATIG WELDING OF FERRITIC STAINLESS STEELS

T. Sándor¹, J. Dobránszky²

¹ESAB Ltd., Hungary, ²Research Group for Metals Technology of the Hungarian Academy of Sciences, Hungary

Abstract

As a consequence of the alloy surcharges of austenitic corrosion resistant steels in the last years more and more attention has been focused on the cheaper ferritic stainless steels. Knowing the weldability problems of the ferritic stainless steels, such as grain growth resulting in low ductility, for instance, the application of the activated TIG (ATIG) welding with its lower heat input and focused arc may provide certain advantages. This paper summaries the experiments performed on ferritic steels with various thickness, welding speeds and heat inputs. Microscopic examinations were also done to compare conventional welding methods and ATIG welding.

Introduction

In the last years an enormous market demand has appeared concerning the stainless steels. Here and usually when we say “stainless” one means “austenitic stainless steel” as 80-90% of the total stainless steel consumption is austenitic. The advantages of austenitic types are very well known: good formability, excellent weldability, good corrosion resistance, decorative outlook, and so on. An additional benefit is that these properties are well documented that helps the user to find out solutions for any problem that may occur during production.

Contrary to austenitics, the ferritic and martensitic types have several problems, which have limited their use. However, in some specific areas these steels may be unique solutions. The most common austenitic stainless steels contain 8-13% Ni. With increasing of alloy surcharges and nickel prices the interest in low-nickel content stainless steels has rapidly increased. Among the duplex steels these types are called “lean duplex”. Parallel with these developments the focus of the market’s attention has turned to ferritic stainless steels (FSSs). This work will present some results regarding the grain coarsening and intergranular corrosion sensitivity of FSSs as welded by the Activated Tungsten Inert Gas (ATIG) method.

ATIG welding

The ATIG welding method is a high productivity variation of conventional TIG welding. When applying this, so far an unfrequently used welding process, welding may be executed with substantially lower welding current and higher welding speed, even though the penetration is 2-3 times deeper compared to that with the conventional TIG welding. When ATIG welding is applied for welding of stainless steels the following should be noticed:

- ATIG welding is applicable without bevelling. This decreases the cost and time of production;
- A gap is not recommended, as it increases the possibility of porosity;
- One size thicker tungsten electrode should be used to resist the higher reflected heat;
- Electrode sharpening should be around 45° for longer life expectancy;

- Consistent active flux portioning is important;
- Any filler metal is (usually) not added to the weld pool.

Main characteristics of ferritic stainless steels

Although FSSs offer many useful properties (formability, good corrosion resistance, high stress corrosion cracking resistance, low thermal coefficient and consequently low thermal fatigue tendency, and low price) unfortunately the user should also be aware of some handicaps:

- Many FSS pass through the γ -loop during cooling, which leads to the formation of austenite and subsequently martensite (Figure 1);
- The presence of even a very low carbon content in FSSs tends to form carbides that finally results in high risk of intergranular corrosion;
- Sensitive to 475°C embrittlement (especially when Cr-content is above 18%); σ -phase can form in the temperature range 500... 800°C (tendency increases with Cr);
- Knife-line corrosion may occur in the heat affected zone (HAZ) in grades stabilised with Nb or Ti;
- Significant grain coarsening in the HAZ decreases the ductility;
- In fully ferritic types, because of the lack of $\gamma \rightarrow \alpha$ transformation, any heat treatment is not possible to refine the coarsened grain structure.

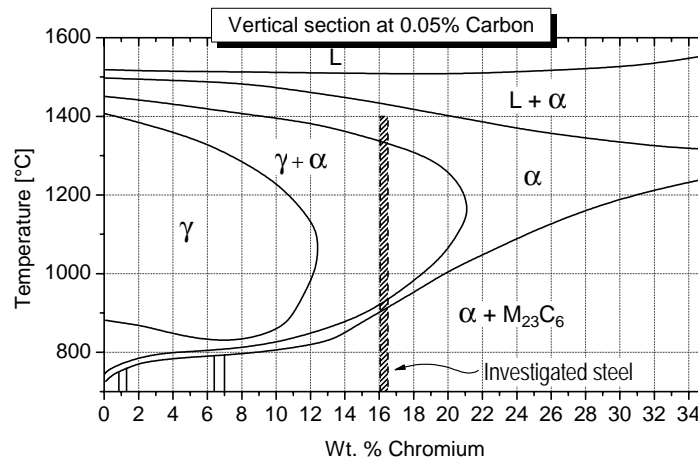


Figure 1. Fe-Cr-C quasi-ternary phase diagram with 0,05%C content [5]

After solidification the FSSs largely keep their body centred cubic lattice (bcc) until the room temperature. This explains why a grain refining heat treatment is not possible for them, and consequently it may be stated that a major disadvantage of FSSs is the grain coarsening in HAZ. This phenomenon substantially decreases the mechanical properties and corrosion resistance. Moreover, if C is present in FSSs, the formation of carbides is almost unavoidable that finally leads to worse mechanical properties and impaired corrosion resistance.

In the following this paper will present the effect of ATIG welding to grain structure of FSSs compared to obtained with the TIG welding. [5], [7], [3]

Experiments

The ATIG welding experiments were carried out in flat butt weld (PA) position without bevelling and without gap. Both shielding and backing gases used were pure argon (T4.5). The arc length (the gap between tungsten electrode and the plate) was kept at 2 mm. A consistent arc length and welding speed were ensured by using a mechanised TIG torch moving table. Here the

constant arc length parallel with the analogue setting of welding speed with a potentiometer was also possible.

The base material was AISI 430 type (X6Cr17; 1.4016; UNS S43000) ferritic stainless steel, with the plate thickness of 8 mm. The chemical composition is given in Table 1.

Table 1. Chemical composition of investigated 430 type ferritic stainless steel.

C	Mn	Si	Cr	P	S
0,046	0,67	0,46	16,36	0,02	0,003

The cut edges were ground manually and cleaned with alcohol to remove any grease or oil residuals in the vicinity of the joint.

The welding parameters were optimised for ATIG welding to obtain absolutely perfect root penetration. The same parameters were applied for TIG welding afterwards to ensure the same heat input. Thus the comparison of TIG and ATIG welding was possible from the point of view of heat input. The measured average grain size of base material was in the range of 30...80 μm . After parameter optimisation, the welding parameters as follows were applied (Table 2).

Table 2. Welding parameters of TIG and ATIG welding of 8 mm thick 430 type ferritic stainless steel.

	Welding current (A)	Voltage (V)	Power (kW)	Arc efficiency (%)	Welding speed (mm/min)	Heat input (kJ/mm)
ATIG welding	240	20,8	5,00	75	70	3,2
TIG welding	240	20,8	5,00	75	70	3,2

Results of TIG welding

As the welding parameters of TIG welding were set for ATIG, naturally a perfect penetration was not expected. Thus, only simple bead-on-plate welds were examined (Figure 2).



Figure 2. A cross-section of bead-on-plate welded with TIG process; weld penetration less than 3 mm.

As in the 430 type FSS examined the carbon content was 0.046%, according to Figure 1 austenite and optionally martensite formation were expected. Consequently, the most interesting questions were how much the grain size increased due to the 3.2 kJ/mm heat input in the HAZ and how much austenite/martensite formed in the welded metal and in the HAZ. As expected, the grain coarsening was significant (Figure 3) in the HAZ. The average grain size increased to the range of 60...120 μm .

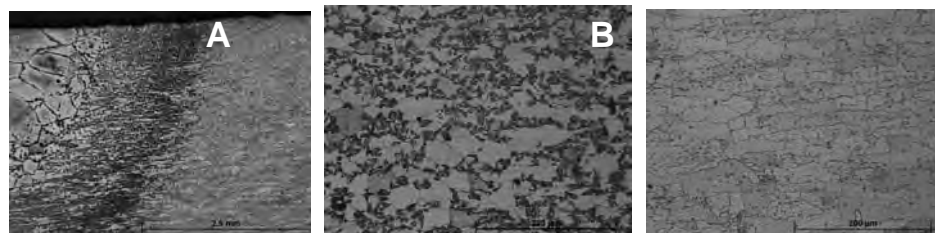


Figure 3. Macro- (A) and microstructure (B) of the HAZ of TIG-welded joint and the base material (C).

The tremendous grain size increase in the weld metal might have been less pronounced with a lower heat input, but this was outside the scope of this investigation. [6]

Results of ATIG welding

The joints made with the ATIG welding, using the parameters listed in Table 2, showed a complete root penetration (Figure 4).



Figure 4. A cross-section of ATIG welded joint; plate thickness 8 mm.

The cross-sections of the joint indicate that the welding current used could be slightly lower. However, a somewhat higher current was necessary to avoid root penetration faults owing to a not absolutely perfect fitting. The most interesting observation when comparing HAZ and fused weld metals of TIG and ATIG was that in the case of ATIG welding less grain coarsening and more martensite formation were present. This originates from the fact that the weld pool of TIG is more shallow, so that the arc energy heats up the weld pool to a higher temperature. Therefore grains have more time to grow in the HAZ while they are in the critical temperature range for a longer time. In the case of ATIG welding the weld pool is deeper and the volume of molten metal is larger. Therefore the arc energy does not heat up the weld pool to the same extent and the HAZ (and the weld pool) can cool down faster through the critical temperature range, which results in a finer grain structure [8]. The faster cooling rate increases the possibility of formation of martensite. The difference in the martensite contents is shown in Figure 5.

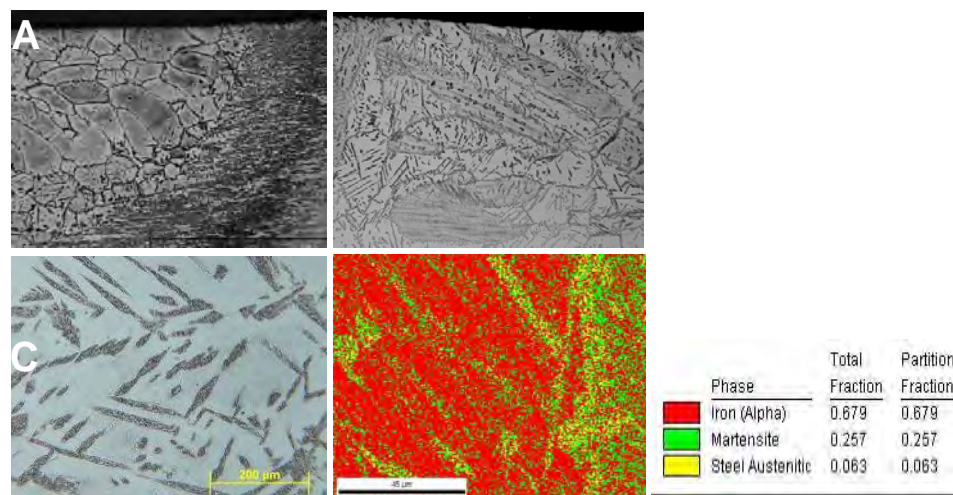


Figure 5. Microstructures of ATIG (A) and TIG welded joint (B). Acicular plates in ferrite matrix of the ATIG welded joint (C) and phase map of an interior part of a plate (D)

EBSD analysis and microhardness testing on the grain boundaries were used to examine the austenite/martensite ratio. The EBSD stated that the austenite/martensite ratio was slightly bigger in the TIG welded joint, corresponding to its lower cooling rate, while the martensite fraction was bigger in the ATIG welded joint. The microhardness testing showed that in both cases the

austenite decreased the hardness of the martensite. While the hardness was 170-175 HV_{0,05} inside the ferritic grains, it was 270-320 HV_{0,05} at the grain boundaries (the hardness of martensite is over 400-500 HV).

Reducing the heat input can decrease the grain size of both the welded joint and the HAZ. This can be achieved by reducing the welding current or increasing the welding speed. By applying these techniques the penetration of the joint will not be sufficient. Therefore, a two-sided technique was applied.

Results of two-sided ATIG welding

The two-sided technique was applied following the same guidelines as described in the introduction. Two-sided welding have many advantages:

- no need of backing gas;
- no need of precise parameter setting (as there was no chance of burn through);
- no need of accurate fitting of the plates.

In view of these points the following (Table 3) parameters were employed to achieve the full penetration.

Table 3. Welding parameters for two-sided ATIG welding.

	Welding current (A)	Voltage (V)	Power (kW)	Arc efficiency (%)	Welding speed (mm/min)	Heat input (kJ/mm)
Two-sided ATIG welding	240	20,8	5	75	150	1,5

Most of the international literature states that to minimise the grain coarsening in FSSs during welding, the heat input as low as possible should be maintained. Thus, naturally significantly lower grain coarsening was expected in both HAZ and welded joint in two-sided welding. No welding defects appeared in the joint with special regards to the remelted zone (Figure 6A). However, the expectations were not completely fulfilled. As is seen in Figure 6B and 6C, only a very slight decrease of the HAZ width was achieved and the austenite + martensite formation was not avoided.



Figure 6. A) The joint of two-sided ATIG joint; B) HAZ of two-sided ATIG joint; C) HAZ of TIG joint.

Conclusions

On the basis of the experimental work the following conclusions can be stated:

- The lower heat input cannot avoid the formation of austenite, martensite and carbides in 430 type FSS. Hence, the welding of this type FSS is not recommended, not even by the ATIG process.
- By application of ATIG welding instead of conventional TIG with a given heat input, faster cooling can be reached producing slightly more martensite on grain boundaries.
- Single-pass welding of 8 mm thick FSSs is not possible using the heat input below ~3 kJ/mm, neither with TIG nor with ATIG welding.

- The heat input can be decreased and productivity can be increased substantially by two-sided welding applying the ATIG method.
- Further mechanical testing is required to evaluate these results from practical points of view.

References

- [1] K. Bődök: “The corrosion resistance of mild, low alloy and high alloy structural steels with special attention to their weldability”, Corweld, Budapest 1997.
- [2] CIGWELD: “Technical and trade information – Welding of stainless steels”, Comweld Group Pty Ltd., 2000.
- [3] J. R. Davis: ASM Specialty Handbook – Stainless steels, ASM International Materials Park, OH 440730002, 1999.
- [4] ESAB: “Repair and maintenance welding handbook”, 3rd edition, Gothenburg, Sweden, 1995.
- [5] M. van Warmelo, D. Nolan, J. Norrish: “Mitigation of sensitisation effects in unstabilised 12% Cr ferritic stainless steel welds”, Materials Science and Engineering A, 464 (2007), pp. 157-169.
- [6] J. D. Verhoeven: “Metallurgy of steel for bladesmith and others who heat treat and forge steel”, Iowa state University, March, 2005.
- [7] L. de A. Silva, L. I. L. Lima, W. R. da C. Campos: “Microstructural characterization of the HAZ of the AISI 439 with different heat input”, INAC 2007, Santos, SP, Brazil, 30 of September to 5th of October in 2007.
- [8] Atlas Specialty Metals Technical Services Department: “Technical Handbook of Stainless steels”, July, 2003, http://www.atlasmets.com.au/files/technical_handbook.pdf. (16-02-2008).
- [9] J. J. Lowke, M. Tanaka, M. Ushio: “Mechanisms giving increased weld depth due to a flux”, Journal of Physics D: Applied Physics, 38 (2005), pp. 3438-3445.
- [10] L. Béres, M. Komócsin: “Repair and maintenance welding of steels and cast irons”, Budapest, 1995.
- [11] V. F. Zackay, H. I. Aaronson (eds.): “Decomposition of austenite by diffusional processes.” Proceedings of the symposium of the Metallurgical Society of AIME Ferrous Metallurgy Committee, held in Philadelphia, Pennsylvania, October 19, 1960, Interscience Publishers, Inc. / John Wiley & Sons, New York - London 1962. pp. 387-545.